ACS APPLIED NANO MATERIALS

www.acsanm.org Article

Microscopic Linker Distribution in Mixed-Linker Zeolitic Imidazolate Frameworks via Computational Raman Spectroscopy: Implications for Gas Separation

Alexander E. J. Hoffman, João Marreiros, Sven M. J. Rogge, Rob Ameloot, and Veronique Van Speybroeck*

Cite This: *ACS Appl. Nano Mater.* 2023, 6, 5645−5652 Read Online

ACCESS | Metrics & More | Article Recommendations | Supporting Information

ABSTRACT: Mixed-linker zeolitic imidazolate frameworks (ZIFs) are important candidate materials for gas separation. By changing the linker content, their pore size can be tuned, offering the potential to regulate diffusion and adsorption. An important factor affecting these properties in mixed-linker ZIFs is the linker distribution, which is difficult to characterize. In this study, the microscopic linker distribution in mixed-linker ZIF-8/ZIF-90, with respectively methyl and carboxaldehyde functionalization, is elucidated via computational Raman spectroscopy. It is shown that the typical Raman band associated with the carboxaldehyde linker is shifted due to a change in hydrogen-bonding behavior. This insight allows one to explain the microscopic linker distribution in experimental mixed-linker structures.

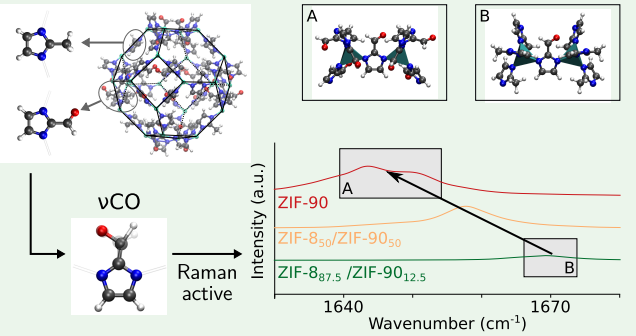

KEYWORDS: *zeolitic imidazolate framework, mixed linker, microscopic linker distribution, Raman spectroscopy, ab initio molecular dynamics, radial distribution function, hydrogen bonds*

INTRODUCTION

Metal−organic frameworks (MOFs) are micro- and/or nanoporous crystalline materials consisting of a net of inorganic polynuclear clusters connected by organic linkers.[1−3] Reticular chemistry enables one to tune this net by using different organic and inorganic building blocks, leading to a vast number of different MOFs.[4,5] In particular, this building block concept allows one to design mixed-linker MOFs with possibly superior properties over the parent single-linker structures.[6−9] Furthermore, the mixing of linkers facilitates the tuning of specific material properties toward applications of interest. For example, mixed-linker MOFs have proven to be beneficial in catalysis,[10−12] photocatalysis,[13−15] light harvesting,[16] thermal expansion tuning,[17] and gas separation.[18]

A subclass of MOFs is formed by zeolitic imidazolate frameworks (ZIFs). These are topologically identical with zeolites in which silicon has been replaced by metal ions such as Zn^{2+} and the function of the bridging oxygen atoms has been taken over by imidazolate linkers.[19,20] ZIFs are particularly interesting materials for gas separation because they usually combine high permeability and attractive selectivity.[21] Moreover, they have relatively high thermal and chemical stability.[19] ZIF-8, in particular, has been frequently investigated due to its interesting diffusion properties (e.g., a pore limiting diameter of 3.4 Å) for small molecules such as H_2 and CO_2.[22,23] Each single-linker ZIF has only a limited number of possible kinetic separations because the process is extremely sensitive to changes in the effective pore size. Moreover, creating an entirely different ZIF for each new separation task is cumbersome. Through the design of mixed-linker ZIFs, the effective pore size can be tuned in a more systematic way, offering the possibility to regulate the diffusion and adsorption properties.[24−29]

An important factor that affects the properties of mixed-linker ZIFs is the distribution of linkers within the crystal. Macroscopically, two different situations can be distinguished. On the one hand, the different linkers may be spread out more or less homogeneously throughout the crystal, which frequently arises after *de novo* synthesis of the material.[30] On the other hand, linkers of the same type can have a tendency to cluster together in separate domains, which is often the case after postsynthetic linker exchange.[31,32] Nevertheless, in order to understand the diffusion properties of mixed-linker ZIFs,

Received: January 8, 2023
Accepted: March 17, 2023
Published: March 29, 2023

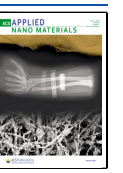

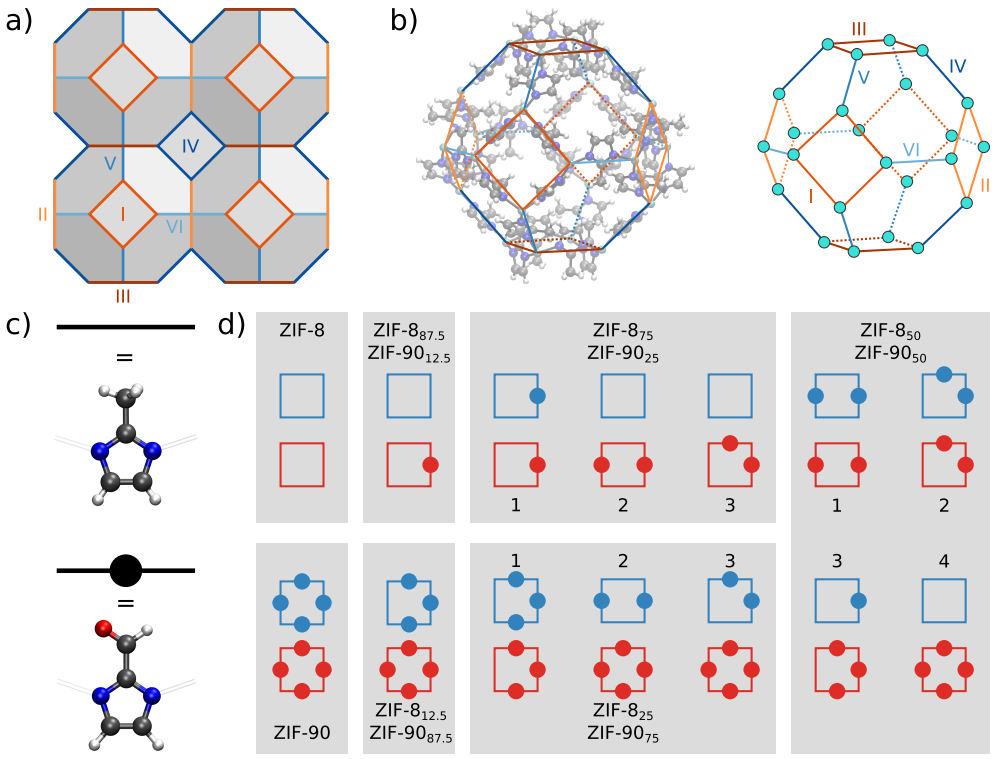

Figure 1. (a) Visualization of the SOD topology. The two mutually exclusive sets of 4-rings are sketched in red/orange (rings I−III) and blue (rings IV−VI) colors, respectively. (b) Unit cell of ZIF-8 with schematic visualization of the two sets of 4-rings: three 4-rings with red/orange colors (rings I−III) and three 4-rings with blue colors (rings IV−VI). (c) Illustration of the mIm (left) and ICA (right) linkers. (d) Schematic visualization of the linker distribution in the two different single-linker and 12 different mixed-linker configurations considered in this study. In a single configuration, each of the three 4-rings of the same set (blue or red) has an identical distribution. For configurations with 25%/75% and 50%/50% linker mixtures, three and four different distributions, respectively, are considered.

there is a need to acquire microscopic insight, i.e., how the linkers are distributed at the unit-cell level. The microscopic linker distribution will directly affect the pore sizes and shapes and, hence, determine the diffusion rate. Earlier reports use NMR techniques to obtain such local information.[30,33] However, it is not always possible to obtain a detailed molecular-level insight when relying only on those spectroscopic techniques.[32]

Here, we demonstrate that computational Raman spectroscopy is ideally placed to elucidate the microscopic linker distribution in mixed-linker ZIF-8/ZIF-90 configurations. ZIF-8 and ZIF-90 both have a sodalite (SOD) topology in which the Zn^{2+} ions are tetrahedrally linked by functionalized imidazolate linkers (Figure 1a,b). In ZIF-8, the functionalization consists of a methyl group, leading to 2-methylimidazolate (mIm) linkers.[19,34] In ZIF-90, the mIm linker has been replaced by imidazole-2-carboxaldehyde (ICA)[35] (Figure 1c). The Raman spectrum of ZIF-90 is characterized by a strong Raman band due to stretching of the C═O bond. Experimentally, it has already been observed that, when mixing ICA with mIm in the SOD topology, the Raman band of the latter vibration shifts depending on the linker distribution.[25,32] Our density functional theory (DFT) calculations rationalize this shift and show that it is a function of the environment of the ICA linker. The obtained unit-cell level insight allows one to interpret the microscopic linker distribution in mixed-linker ZIF-8/ZIF-90 structures. Furthermore, it showcases that Raman spectroscopy is ideally suited to characterize materials with different mixed-linker distributions, which are important to tune for gas separation.

METHODS

For all structures, *ab initio* molecular dynamics (AIMD) simulations have been performed with the *CP2K* software[36] at a temperature of 300 K and with a time step of 0.5 fs. Initially, a simulation of 10 ps has been conducted in the *NPT* ensemble after an equilibration run of 5 ps. Subsequently, the average volume was determined and used as the volume of the cubic unit cell for a 5 ps equilibration run and a 20 ps production run in the *NVT* ensemble. These proved to be sufficiently long for the purpose of this study (Figures S1−S3). Afterward, the radial distribution functions (RDFs) and Raman spectra were obtained from the latter. Raman spectra were calculated via discrete Fourier transforms of specific autocorrelation functions of the polarizability tensor.[37] The polarizability tensor was derived every 2 fs via finite differences of the dipole moments with and without an electric field.[37,38] All simulations were performed with the Quickstep module of *CP2K*[36] at the PBE-D3(BJ) level of theory[39−41] with a Gaussian and plane-wave basis set.[42] The plane-wave cutoff was set at 600 Ry, whereas the TZVP MOLOPT basis set[43] was chosen as the atomic basis set, and GTH pseudopotentials[44] were selected. The temperature was controlled by a chain of five Nosé−Hoover thermostats with a time constant of 100 fs.[45] The pressure in the *NPT* run was controlled at 1 bar with a MTK barostat with a time constant of 1 ps.[46]

RESULTS AND DISCUSSION

To investigate the effect of the microscopic linker distribution on the Raman spectrum of mixed-linker ZIF-8/ZIF-90, an accurate theoretical model is required. Therefore, different mixed-linker configurations are constructed at the unit-cell level for which the Raman spectrum is calculated. Because the unit cell consists of 24 linker positions, which might be occupied by either mIm or ICA, a very large number of unique

https://doi.org/10.1021/acsanm.3c00106
ACS Appl. Nano Mater. 2023, 6, 5645−5652

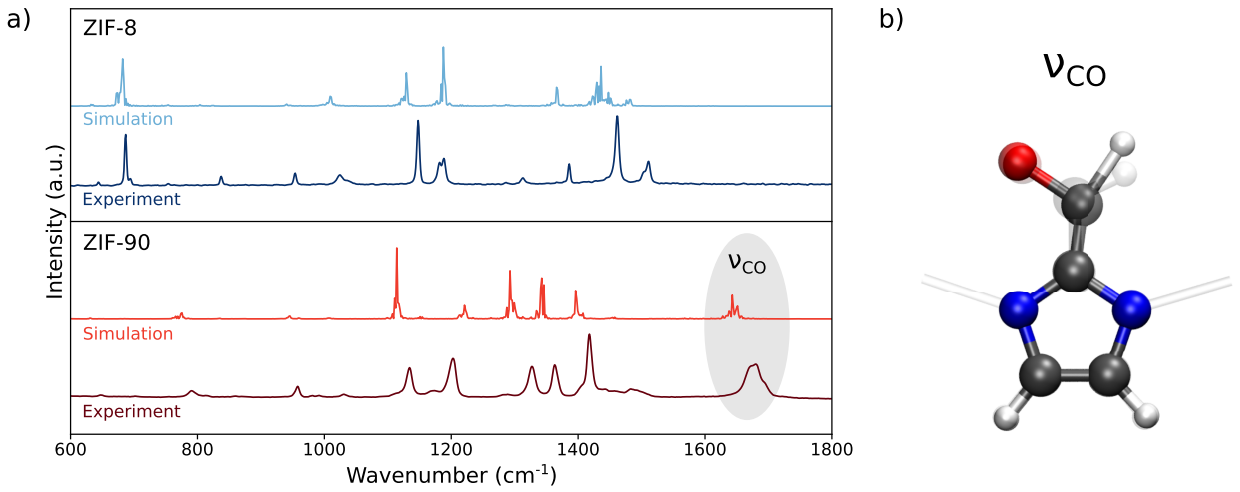

Figure 2. (a) Theoretical and experimental Raman spectra of ZIF-8 and ZIF-90 in the range 600−1800 cm^{-1}. The stretching vibration of the C═O bond (ν_{CO}) in ZIF-90 is highlighted. The experimental Raman data were originally reported in ref 32. (b) Visualization of the ν_{CO} vibration.

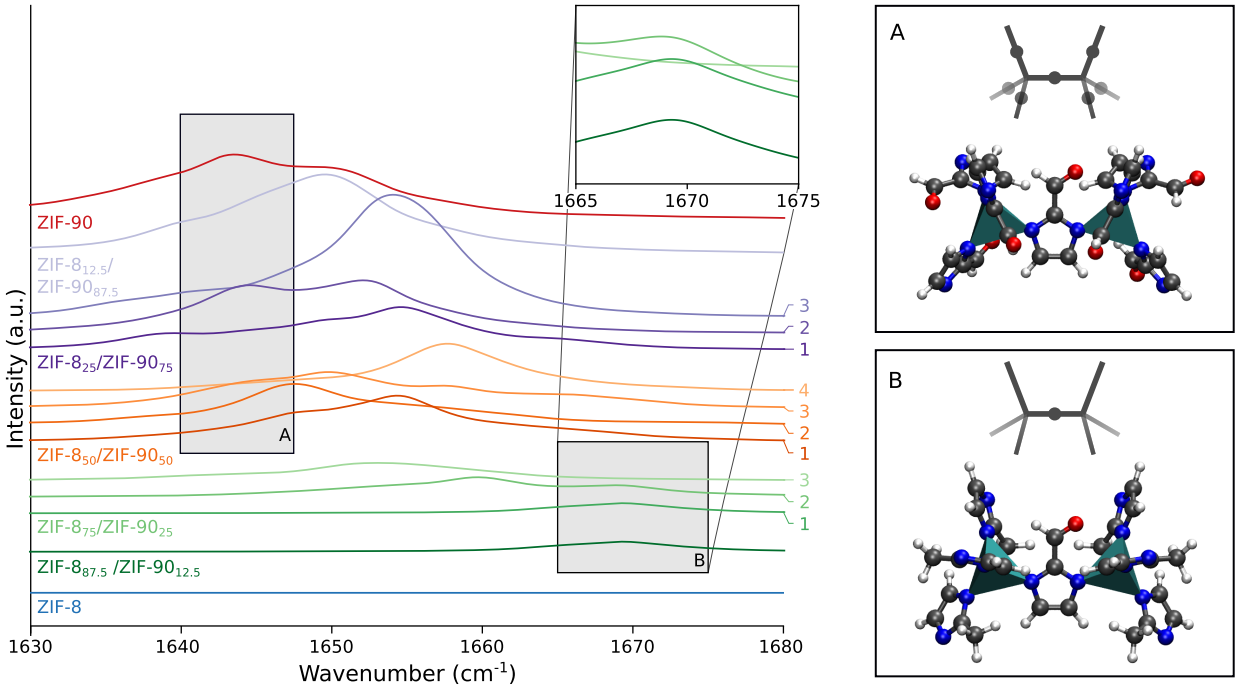

Figure 3. Theoretical Raman spectra of mixed-linker ZIF-8/ZIF-90 structures zoomed in on the C═O stretching region in the range 1630−1680 cm^{-1}. Box A (box B) highlights Raman bands with the lowest (highest) wavenumbers originating from a C═O bond with mainly ICA (mIm) linkers as nearest neighbors. The different mixed-linker structures are labeled according to the scheme in Figure 1d. The Raman spectra of ZIF-8 and ZIF-90 are the same as those reported in Figure 1 except for additional broadening. All spectra were artificially broadened with a Lorentzian line shape with a full-width at half-maximum of 6 cm^{-1} to clearly identify the shift.

combinations exist. It is computationally unfeasible to take all configurations into account. Consequently, to limit the computational cost, a balanced set of 12 distinctly different mixed-linker configurations is selected by carefully inspecting the building pattern of the SOD topology. The unit cell contains two sets of 4-rings, where each set consists of three 4-rings that have no zinc atoms in common. These are indicated in orange/red (rings I−III) and blue (rings IV−VI) in Figure 1a,b. Furthermore, both sets are mutually exclusive in the sense that they do not share linkers. When the mIm and ICA linkers are distributed over the unit cell, all 4-rings of a single set are assumed to have an identical composition, whereas 4-rings of different sets may be constructed differently. Following this rationale and taking into account that the two sets of 4-rings are indistinguishable, there remain only 128 unique configurations. The 14 configurations (including pure ZIF-8 and ZIF-90) that were retained in this study are schematically sketched in Figure 1d with adequate terminology. Their stability with respect to the electronic energy is discussed in Section S2. The selected configurations form a diverse set of structures (see also Section S3), which should allow for a thorough analysis of the direct linker environment on the spectroscopic features.

Before analysis of the Raman fingerprints of the mixed-linker configurations, it is required to assess the performance of our theoretical methodology in predicting the experimental Raman

https://doi.org/10.1021/acsanm.3c00106
ACS Appl. Nano Mater. 2023, 6, 5645−5652

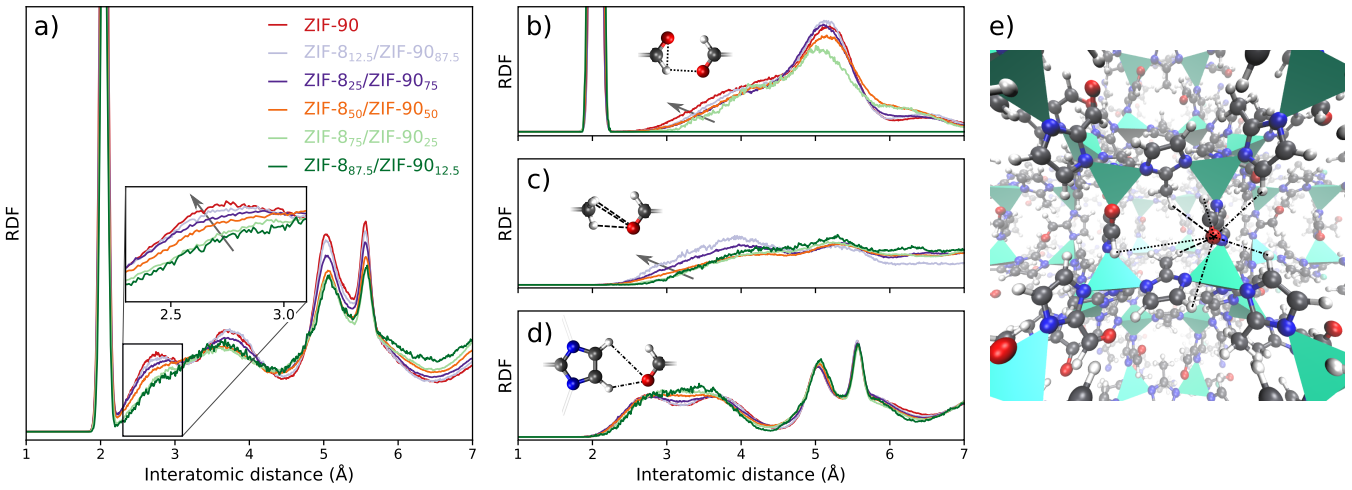

Figure 4. (a) RDF of the OH distances between 1 and 7 Å in ZIF-90 and the different mixed-linker structures. For configurations with 25%/75% and 50%/50% linker mixtures, the average over three and four different distributions, respsectively, is considered. (b–d) RDFs of distances between specific hydrogen atoms [on the carboxaldehyde group (b), on the methyl group (c), and on the imidazolate ring (d)] and the carboxaldehyde oxygen atom. (e) Visualization of the different OH distances on a snapshot of configuration 1 of ZIF-8$_{50}$/ZIF-90$_{50}$.

spectra of the pure ZIF-8 and ZIF-90 structures (Figure 2a). For both materials, a good agreement is achieved for most of the Raman spectral features. The theoretical spectrum (see the Methods section) is globally shifted compared to the experiment, which is an inherent effect of the applied DFT functional.[47] In this case, the PBE-D3(BJ) level of theory has been employed, which has been proven to provide accurate results in the study of MOFs.[48] Because only the theoretical Raman spectra of the mixed-linker configurations will be of interest in the following, no scaling factor has been applied here. Furthermore, in the simulated spectrum of ZIF-90, a single Raman band around 1200 cm^{-1} is shifted to higher wavenumbers with respect to the experimental data. The underlying normal mode induces a deformation of the imidazolate ring due to stretching within the N–C–N unit, as assigned by Eum et al.[25] The respective normal mode is also Raman-active in ZIF-8, but in this case, its frequency is well predicted by theory. All other Raman bands are correctly simulated, proving the validity of our DFT model. In particular, the simulations do reproduce the C═O stretching band of the carboxaldehyde group (ν_{CO}, between 1600 and 1700 cm^{-1}), which is characteristic for the ICA linker and has experimentally been shown to shift upon linker mixing (Figure 2b).[25,32]

Figure 3 shows the theoretically predicted Raman fingerprints in the typical C═O stretching region (from 1630 to 1680 cm^{-1}) for the different mixed-linker structures of Figure 1d. In general, increasing the amount of ICA linker reduces the vibrational frequency of the mode. In the most extreme case of ZIF-90, where all linkers are of the ICA type, the frequency is found around 1645 cm^{-1} (see region A in Figure 3), which is about 25 cm^{-1} lower than those for configurations with low concentrations of the ICA linker (see region B and the inset in Figure 3). Whereas the frequency shift of the ν_{CO} band was already observed experimentally,[25,32] no clear interpretation on the molecular-level origin leading to this effect could be given. Using our DFT model, this frequency shift can now be explained by looking at the surroundings of the respective carboxaldehyde group. On the one hand, the configurations yielding the absolute highest vibrational frequencies contain ICA linkers with only mIm linkers as nearest neighbors (see inset B in Figure 3). This is primarily the case for the ZIF-8$_{87.5}$/ZIF-90$_{12.5}$ structure containing three ICA linkers in the unit cell (one in a single set of 4-rings) but also for two of the ZIF-8$_{75}$/ZIF-90$_{25}$ structures that have (nearly) isolated ICA linkers, yielding Raman bands at high frequency. On the other hand, the lowest vibrational frequencies are found in configurations in which the carboxaldehyde group is surrounded by mainly ICA linkers (see inset A in Figure 3), which is the case for ZIF-90 but also for mixed-linker configurations with 75 and 87.5% of ICA linkers. When the immediate surroundings of the carboxaldehyde group are a mixture of both mIm and ICA linkers, the vibrational frequency of ν_{CO} takes on intermediate values.

By now it is already clear that the shift of the ν_{CO} vibrational frequency depends on the direct environment of the carboxaldehyde group. The lower vibrational frequency in an ICA environment is an indication that the strength of the C═O bond is weakened by increased dispersive interactions, mainly hydrogen bonds. This can be investigated in more detail by looking at the RDFs of the interatomic distances between the carboxaldehyde oxygen atom and all hydrogen atoms (Figure 4). The strength of the hydrogen bonds strongly depends on the distance between the involved atoms. Hence, the RDF forms a good measure to estimate the influence of hydrogen bonds on the strength of the C═O bond.

The RDFs with OH interatomic distances in the range of 1–7 Å exhibit a sharp peak around 2 Å, indicative for the distance between the oxygen and hydrogen atom on the same carboxaldehyde group. Furthermore, two sharp peaks can be observed around 5 and 5.5 Å, which can be assigned to the distances of the oxygen atom and the two hydrogen atoms on the imidazolate ring of the same ICA linker. The other RDF features are broader and correspond to OH distances of the oxygen atom and hydrogen atoms on neighboring ICA and mIm linkers. To reveal information on the molecular environment of the ICA linkers, it is most important to focus on the features below 3 Å, which can have a significant contribution to the hydrogen bonds. Between 2 and 3 Å, a single RDF peak can be distinguished that becomes more pronounced and shifts to lower interatomic distances in configurations with larger concentrations of ICA linkers (see

https://doi.org/10.1021/acsanm.3c00106
ACS Appl. Nano Mater. 2023, 6, 5645–5652

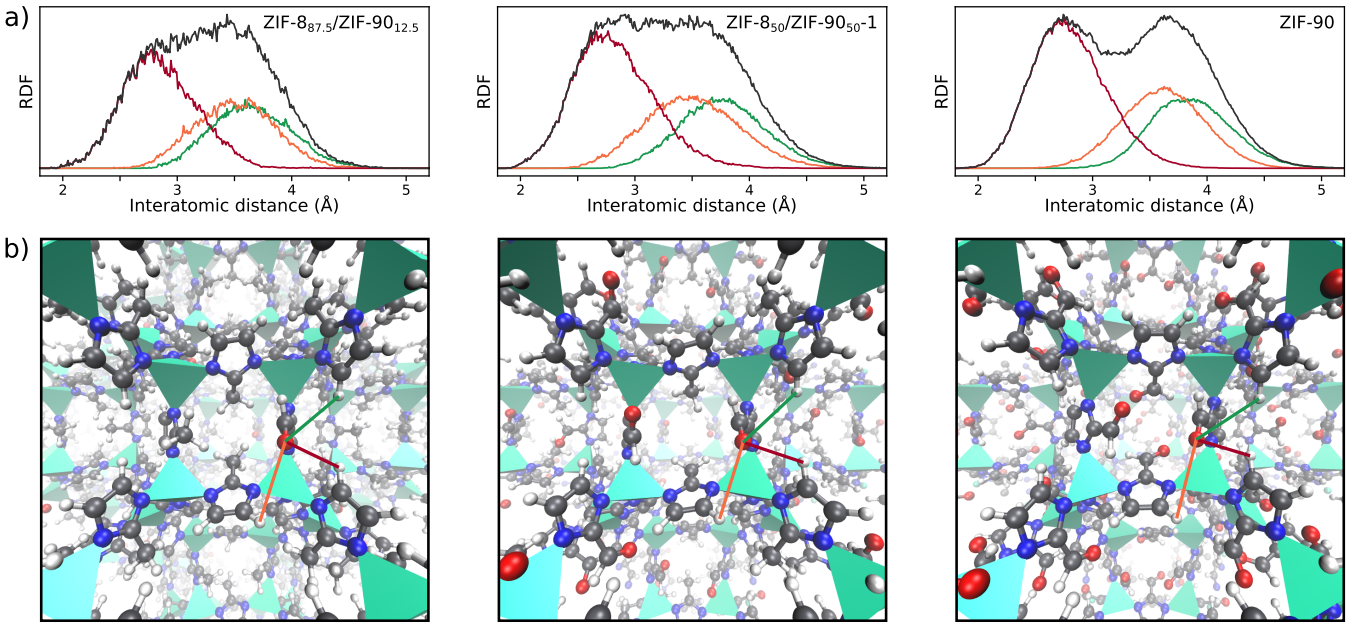

Figure 5. (a) RDFs of the OH distances between the oxygen atom and its three nearest hydrogen atoms on the imidazolate rings in ZIF-8$_{87.5}$/ZIF-90$_{12.5}$, configuration 1 of ZIF-8$_{50}$/ZIF-90$_{50}$, and ZIF-90. (b) Visualization of these OH distances in snapshots of the respective structures.

the inset in Figure 4a). This small shift is an indication that hydrogen bonds become stronger when there are more ICA linkers. The origin of this shift can be explained by analyzing the different contributions to the RDF. On the one hand, OH distances between the oxygen atom and the hydrogen atom(s) on the functional group of the linker on the opposite side of the same 4-ring are shifted toward lower values when the amount of ICA linkers is increased (Figure 4b,c). On the other hand, also the contribution arising from the interatomic distances between the oxygen atom and the hydrogen atoms on the imidazolate rings of neighboring linkers changes (Figures 4d). For the latter, a single broad RDF peak is present between 2 and 4 Å for configurations with low concentrations of ICA linkers. However, by increasing the ICA linker content, the broad RDF peak splits into two separate contributions. More in-depth analysis shows that this feature originates from three different OH distances (Figure 5). The first OH distance (red color in Figure 5) peaks around 2.8 Å and decreases only slightly when more ICA linkers are introduced. In contrast, the second and third OH distances (the orange and green colors, respectively, in Figure 5), with maxima situated above 3.4 Å, increase with increasing ICA linker content. As a result, two separate RDF features can be resolved at high ICA linker concentrations.

Clearly, more ICA linkers lead to a reorientation of the imidazolate linkers, which shortens the OH distances by between 2 and 3 Å, especially the ones between the oxygen atom on the ICA linker and the hydrogen atoms on the functional groups of the neighboring ICA and mIm linkers, leading to stronger hydrogen bonds.

An interesting observation, which has not been mentioned yet, is that the ZIF-90 structure is characterized by multiple Raman bands due to C═O stretching in its theoretical spectrum, in agreement with the experiment.[25,32] This is not trivial because the ICA linkers in ZIF-90 all have the same surroundings. The multiple Raman bands can be linked to the flexibility of the linker. Although the linker orientation in ZIF-90 is more structured than that in the case of ZIF-8, the linker is still relatively flexible. Therefore, it can take multiple orientations, which impact the vibrational frequency of the C═O stretching mode. When the particular orientation gives rise to relatively strong hydrogen bonds, the C═O stretching frequency will be reduced, whereas the opposite is true in the case of weaker hydrogen bonds. If there was only a single preferential orientation, this would give rise to one broad Raman peak. The fact that more than one peak can be observed in the Raman spectrum of ZIF-90 indicates that there are multiple preferred linker orientations that are more probable than others.

As a final note, it has to be clear that the hydrogen-bond strength depends not only on the distance between the oxygen and hydrogen atoms but also on the charges of the involved atoms. However, because the RDFs for the functional group of the mIm linker and the functional group of the ICA linker show the same trends in the distance range in which hydrogen bonds are important, it is not expected to affect the conclusions drawn above.

The above analysis illustrates that the frequency of the ν_{CO} vibration is intimately correlated with the strength of the hydrogen bonds in its immediate surroundings. Accordingly, it can yield direct insight into the microscopic linker distribution within the experimental mixed-linker ZIF-8/ZIF-90. Applied to the work of Eum et al., which reports Raman spectra of mixed-linker materials obtained via direct synthesis,[25] the gradual shift of the ν_{CO} vibration provides an additional confirmation of the homogeneous distribution of the linkers. However, the origin of the Raman shift in the work of Marreiros et al., which measured the Raman spectra of large 150-μm-sized mixed-linker ZIF-8/ZIF-90 crystals obtained after vapor-phase ligand exchange (VPLE),[32] is less easy to understand solely based on our theoretical insights. For these large crystals, NMR results suggest that VPLE creates separate domains of ZIF-8 and ZIF-90. This would mean that the Raman band of the ν_{CO} vibration would not shift when the ratio of the linkers is adapted. Such a shift is observed nevertheless in the Raman spectrum. Possibly, the very large crystal size introduces other effects in the Raman

https://doi.org/10.1021/acsanm.3c00106
ACS Appl. Nano Mater. 2023, 6, 5645−5652

spectrum, which cannot be fully captured by our unit-cell model. This requires supercell structures that can make a distinction between clustered, random, or sparse distributions.[30,49,50] However, such extended structures can no longer be described by *ab initio* methods at the moment, complicating calculation of the Raman intensities. In that regard, the development of machine-learning potentials might form a solution.[51]

CONCLUSIONS

In this work, we have demonstrated the power of computational Raman spectroscopy to explain the microscopic linker distribution in mixed-linker ZIF-8/ZIF-90. Experimentally, a typical shift has already been observed with increasing ICA linker content. However, further interpretation on how the linkers are distributed in the framework could not be given. Here, we show with theoretical Raman spectroscopy that the origin of the shift of the ν_{CO} vibration originates from a change in the hydrogen bonds. More precisely, it was evidenced that an increase in the ICA content leads to a reorganization of the functionalized imidazolate linkers and shorter distances between the hydrogen and oxygen atoms. These manifestations can be attributed to an increased strength of the interlinker hydrogen bonds. The direct connection between the shift of the ν_{CO} vibration and the local arrangement of the linkers allowed for a sound spectroscopic fingerprint of the microscopic linker distribution in experimental mixed-linker ZIF-8/ZIF-90 structures. This may be useful to develop mixed-linker MOFs for gas-separation applications.

ASSOCIATED CONTENT

Data Availability Statement

All structure files and input scripts used to obtain the results are available from the online GitHub repository at https://github.com/AlexanderHoffman/supporting-info.

Supporting Information

The Supporting Information is available free of charge at https://pubs.acs.org/doi/10.1021/acsanm.3c00106.

> Study of the effect of the equilibration time and production run length on theoretical Raman spectra, analysis of the stability of the investigated structures, and assessment of the diversity of the considered mixed-linker configurations (PDF)

AUTHOR INFORMATION

Corresponding Author

Veronique Van Speybroeck − *Center for Molecular Modeling, Ghent University, 9052 Zwijnaarde, Belgium;* orcid.org/0000-0003-2206-178X;
Email: Veronique.VanSpeybroeck@UGent.be

Authors

Alexander E. J. Hoffman − *Center for Molecular Modeling, Ghent University, 9052 Zwijnaarde, Belgium;* orcid.org/0000-0002-1529-4705

João Marreiros − *cMACS, Department of Microbial and Molecular Systems (M2S), Katholieke Universiteit Leuven, 3001 Leuven, Belgium;* Present Address: School of Chemical and Biomolecular Engineering, Georgia Institute of Technology, Atlanta, Georgia 30332, United States; orcid.org/0000-0002-4898-2096

Sven M. J. Rogge − *Center for Molecular Modeling, Ghent University, 9052 Zwijnaarde, Belgium;* orcid.org/0000-0003-4493-5708

Rob Ameloot − *cMACS, Department of Microbial and Molecular Systems (M2S), Katholieke Universiteit Leuven, 3001 Leuven, Belgium;* orcid.org/0000-0003-3178-5480

Complete contact information is available at: https://pubs.acs.org/10.1021/acsanm.3c00106

Notes

The authors declare no competing financial interest.

ACKNOWLEDGMENTS

This work was supported by the Fund for Scientific Research Flanders (FWO) and the Research Board of Ghent University. S.M.J.R. acknowledges funding from the FWO through a postdoctoral fellowship (Grant 12T3522N). The computational resources and services used in this work were provided by the Flemish Supercomputer Center, funded by FWO and the Department of Economy, Science & Innovation, the Flemish Government.

REFERENCES

(1) Furukawa, H.; Cordova, K. E.; O'Keeffe, M.; Yaghi, O. M. The chemistry and applications of metal-organic frameworks. *Science* **2013**, *341*, 1230444.

(2) Jiao, L.; Seow, J. Y. R.; Skinner, W. S.; Wang, Z. U.; Jiang, H.-L. Metal−organic frameworks: Structures and functional applications. *Mater. Today* **2019**, *27*, 43−68.

(3) Zhang, X.; Chen, Z.; Liu, X.; Hanna, S. L.; Wang, X.; Taheri-Ledari, R.; Maleki, A.; Li, P.; Farha, O. K. A historical overview of the activation and porosity of metal−organic frameworks. *Chem. Soc. Rev.* **2020**, *49*, 7406−7427.

(4) Moghadam, P. Z.; Li, A.; Wiggin, S. B.; Tao, A.; Maloney, A. G.; Wood, P. A.; Ward, S. C.; Fairen-Jimenez, D. Development of a Cambridge Structural Database subset: a collection of metal−organic frameworks for past, present, and future. *Chem. Mater.* **2017**, *29*, 2618−2625.

(5) Kalmutzki, M. J.; Hanikel, N.; Yaghi, O. M. Secondary building units as the turning point in the development of the reticular chemistry of MOFs. *Sci. Adv.* **2018**, *4*, eaat9180.

(6) McDaniel, J. G.; Yu, K.; Schmidt, J. R. Microscopic origins of enhanced gas adsorption and selectivity in mixed-linker metal−organic frameworks. *J. Phys. Chem. C* **2013**, *117*, 17131−17142.

(7) Qin, J.-S.; Yuan, S.; Wang, Q.; Alsalme, A.; Zhou, H.-C. Mixed-linker strategy for the construction of multifunctional metal−organic frameworks. *J. Mater. Chem. A* **2017**, *5*, 4280−4291.

(8) Dutta, A.; Pan, Y.; Liu, J.-Q.; Kumar, A. Multicomponent isoreticular metal-organic frameworks: Principles, current status and challenges. *Coord. Chem. Rev.* **2021**, *445*, 214074.

(9) Bhattacharyya, S.; Maji, T. K. Multi-dimensional metal-organic frameworks based on mixed linkers: Interplay between structural flexibility and functionality. *Coord. Chem. Rev.* **2022**, *469*, 214645.

(10) Dhakshinamoorthy, A.; Asiri, A. M.; Garcia, H. Mixed-metal or mixed-linker metal organic frameworks as heterogeneous catalysts. *Catal. Sci. Technol.* **2016**, *6*, 5238−5261.

(11) Kleist, W.; Maciejewski, M.; Baiker, A. MOF-5 based mixed-linker metal−organic frameworks: Synthesis, thermal stability and catalytic application. *Thermochim. Acta* **2010**, *499*, 71−78.

(12) Marx, S.; Kleist, W.; Baiker, A. Synthesis, structural properties, and catalytic behavior of Cu-BTC and mixed-linker Cu-BTC-PyDC in the oxidation of benzene derivatives. *J. Catal.* **2011**, *281*, 76−87.

(13) Patial, S.; Raizada, P.; Hasija, V.; Singh, P.; Thakur, V. K.; Nguyen, V.-H. Recent advances in photocatalytic multivariate metal organic frameworks-based nanostructures toward renewable energy

and the removal of environmental pollutants. *Mater. Today Energy* **2021**, *19*, 100589.
(14) Lin, S.; Cairnie, D. R.; Davis, D.; Chakraborty, A.; Cai, M.; Morris, A. J. Photoelectrochemical alcohol oxidation by mixed-linker metal−organic frameworks. *Faraday Discuss.* **2021**, *225*, 371−383.
(15) Chen, T.-F.; Wang, L.-Y.; Wang, Y.-F.; Gao, H.; He, J.; Wang, G.; Meng, X.-F.; Wu, Y.-S.; Deng, Y.-H.; Wan, C.-Q. Facile strategy for efficient charge separation and high photoactivity of mixed-linker MOFs. *ACS Appl. Mater. Interfaces* **2021**, *13*, 20897−20905.
(16) Jia, J.; Gutiérrez-Arzaluz, L.; Shekhah, O.; Alsadun, N.; Czaban-Jóźwiak, J.; Zhou, S.; Bakr, O. M.; Mohammed, O. F.; Eddaoudi, M. Access to highly efficient energy transfer in metal−organic frameworks via mixed linkers approach. *J. Am. Chem. Soc.* **2020**, *142*, 8580−8584.
(17) Baxter, S. J.; Schneemann, A.; Ready, A. D.; Wijeratne, P.; Wilkinson, A. P.; Burtch, N. C. Tuning thermal expansion in metal−organic frameworks using a mixed linker solid solution approach. *J. Am. Chem. Soc.* **2019**, *141*, 12849−12854.
(18) Lyndon, R.; You, W.; Ma, Y.; Bacsa, J.; Gong, Y.; Stangland, E. E.; Walton, K. S.; Sholl, D. S.; Lively, R. P. Tuning the structures of metal−organic frameworks via a mixed-linker strategy for ethylene/ethane kinetic separation. *Chem. Mater.* **2020**, *32*, 3715−3722.
(19) Park, K. S.; Ni, Z.; Côté, A. P.; Choi, J. Y.; Huang, R.; Uribe-Romo, F. J.; Chae, H. K.; O'Keeffe, M.; Yaghi, O. M. Exceptional chemical and thermal stability of zeolitic imidazolate frameworks. *Proc. Nat. Acad. Sci.* **2006**, *103*, 10186−10191.
(20) Chen, B.; Yang, Z.; Zhu, Y.; Xia, Y. Zeolitic imidazolate framework materials: recent progress in synthesis and applications. *J. Mater. Chem. A* **2014**, *2*, 16811−16831.
(21) Zhang, C.; Koros, W. J. Zeolitic imidazolate framework-enabled membranes: challenges and opportunities. *J. Phys. Chem. Lett.* **2015**, *6*, 3841−3849.
(22) Hertäg, L.; Bux, H.; Caro, J.; Chmelik, C.; Remsungnen, T.; Knauth, M.; Fritzsche, S. Diffusion of CH_4 and H_2 in ZIF-8. *J. Membr. Sci.* **2011**, *377*, 36−41.
(23) Chen, C.; Ozcan, A.; Yazaydin, A. O.; Ladewig, B. P. Gas permeation through singlecrystal ZIF-8 membranes. *J. Membr. Sci.* **2019**, *575*, 209−216.
(24) Thompson, J. A.; Blad, C. R.; Brunelli, N. A.; Lydon, M. E.; Lively, R. P.; Jones, C. W.; Nair, S. Hybrid zeolitic imidazolate frameworks: controlling framework porosity and functionality by mixed-linker synthesis. *Chem. Mater.* **2012**, *24*, 1930−1936.
(25) Eum, K.; Jayachandrababu, K. C.; Rashidi, F.; Zhang, K.; Leisen, J.; Graham, S.; Lively, R. P.; Chance, R. R.; Sholl, D. S.; Jones, C. W.; Nair, S. Highly tunable molecular sieving and adsorption properties of mixed-linker zeolitic imidazolate frameworks. *J. Am. Chem. Soc.* **2015**, *137*, 4191−4197.
(26) Hou, Q.; Wu, Y.; Zhou, S.; Wei, Y.; Caro, J.; Wang, H. Ultra-tuning of the aperture size in stiffened ZIF-8_Cm frameworks with mixed-linker strategy for enhanced CO_2/CH_4 separation. *Angew. Chem., Int. Ed.* **2019**, *58*, 327−331.
(27) Ding, R.; Zheng, W.; Yang, K.; Dai, Y.; Ruan, X.; Yan, X.; He, G. Amino-functional ZIF-8 nanocrystals by microemulsion based mixed linker strategy and the enhanced CO_2/N_2 separation. *Sep. Purif. Technol.* **2020**, *236*, 116209.
(28) Åhlén, M.; Jaworski, A.; Strømme, M.; Cheung, O. Selective adsorption of CO_2 and SF_6 on mixed-linker ZIF-7−8s: The effect of linker substitution on uptake capacity and kinetics. *Chem. Eng. J.* **2021**, *422*, 130117.
(29) Utpalla, P.; Mor, J.; Sharma, S. K.; Bahadur, J.; Pujari, P. K. Pore interconnectivity and surface accessibility in stiffened mixed linker MOFs: An investigation using variable energy positron spectroscopy. *J. Solid State Chem.* **2022**, *307*, 122738.
(30) Jayachandrababu, K. C.; Verploegh, R. J.; Leisen, J.; Nieuwendaal, R. C.; Sholl, D. S.; Nair, S. Structure elucidation of mixed-linker zeolitic imidazolate frameworks by solidstate ^{1}H CRAMPS NMR spectroscopy and computational modeling. *J. Am. Chem. Soc.* **2016**, *138*, 7325−7336.
(31) Jayachandrababu, K. C.; Sholl, D. S.; Nair, S. Structural and mechanistic differences in mixed-linker zeolitic imidazolate framework synthesis by solvent assisted linker exchange and de novo routes. *J. Am. Chem. Soc.* **2017**, *139*, 5906−5915.
(32) Marreiros, J.; Van Dommelen, L.; Fleury, G.; de Oliveira-Silva, R.; Stassin, T.; Iacomi, P.; Furukawa, S.; Sakellariou, D.; Llewellyn, P. L.; Roeffaers, M.; Ameloot, R. Vapor-phase linker exchange of the metal−organic framework ZIF-8: a solvent-free approach to post-synthetic modification. *Angew. Chem., Int. Ed.* **2019**, *58*, 18471−18475.
(33) Kong, X.; Deng, H.; Yan, F.; Kim, J.; Swisher, J. A.; Smit, B.; Yaghi, O. M.; Reimer, J. A. Mapping of functional groups in metal-organic frameworks. *Science* **2013**, *341*, 882−885.
(34) Huang, X.-C.; Lin, Y.-Y.; Zhang, J.-P.; Chen, X.-M. Ligand-directed strategy for zeolite-type metal−organic frameworks: zinc (II) imidazolates with unusual zeolitic topologies. *Angew. Chem., Int. Ed.* **2006**, *45*, 1557−1559.
(35) Morris, W.; Doonan, C. J.; Furukawa, H.; Banerjee, R.; Yaghi, O. M. Crystals as molecules: postsynthesis covalent functionalization of zeolitic imidazolate frameworks. *J. Am. Chem. Soc.* **2008**, *130*, 12626−12627.
(36) Kühne, T. D.; Iannuzzi, M.; Del Ben, M.; Rybkin, V. V.; Seewald, P.; Stein, F.; Laino, T.; Khaliullin, R. Z.; Schütt, O.; Schiffmann, F.; Golze, D.; Wilhelm, J.; Chulkov, S.; Bani-Hashemian, M. H.; Weber, V.; Borštnik, U.; Taillefumier, M.; Jakobovits, A. S.; Lazzaro, A.; Pabst, H.; Müller, T.; Schade, R.; Guidon, M.; Andermatt, S.; Holmberg, N.; Schenter, G. K.; Hehn, A.; Bussy, A.; Belleflamme, F.; Tabacchi, G.; Glöß, A.; Lass, M.; Bethune, I.; Mundy, C. J.; Plessl, C.; Watkins, M.; VandeVondele, J.; Krack, M.; Hutter, J. CP2K: An electronic structure and molecular dynamics software package - Quickstep: Efficient and accurate electronic structure calculations. *J. Chem. Phys.* **2020**, *152*, 194103.
(37) Thomas, M.; Brehm, M.; Fligg, R.; Vöhringer, P.; Kirchner, B. Computing vibrational spectra from ab initio molecular dynamics. *Phys. Chem. Chem. Phys.* **2013**, *15*, 6608−6622.
(38) Lezcano-Gonzalez, I.; Campbell, E.; Hoffman, A. E. J.; Bocus, M.; Sazanovich, I. V.; Towrie, M.; Agote-Aran, M.; Gibson, E. K.; Greenaway, A.; De Wispelaere, K.; Van Speybroeck, V.; Beale, A. M. Insight into the effects of confined hydrocarbon species on the lifetime of methanol conversion catalysts. *Nat. Mater.* **2020**, *19*, 1081−1087.
(39) Perdew, J. P.; Burke, K.; Ernzerhof, M. Generalized gradient approximation made simple. *Phys. Rev. Lett.* **1996**, *77*, 3865.
(40) Grimme, S. Semiempirical GGA-type density functional constructed with a long-range dispersion correction. *J. Comput. Chem.* **2006**, *27*, 1787−1799.
(41) Grimme, S.; Ehrlich, S.; Goerigk, L. Effect of the damping function in dispersion corrected density functional theory. *J. Comput. Chem.* **2011**, *32*, 1456−1465.
(42) Lippert, G.; Hutter, J.; Parrinello, M. A hybrid Gaussian and plane wave density functional scheme. *Mol. Phys.* **1997**, *92*, 477−488.
(43) VandeVondele, J.; Hutter, J. Gaussian basis sets for accurate calculations on molecular systems in gas and condensed phases. *J. Chem. Phys.* **2007**, *127*, 114105.
(44) Goedecker, S.; Teter, M.; Hutter, J. Separable dual-space Gaussian pseudopotentials. *Phys. Rev. B* **1996**, *54*, 1703.
(45) Martyna, G. J.; Klein, M. L.; Tuckerman, M. Nosé−Hoover chains: The canonical ensemble via continuous dynamics. *J. Chem. Phys.* **1992**, *97*, 2635−2643.
(46) Martyna, G. J.; Tobias, D. J.; Klein, M. L. Constant pressure molecular dynamics algorithms. *J. Chem. Phys.* **1994**, *101*, 4177−4189.
(47) Hoffman, A. E. J.; Vanduyfhuys, L.; Nevjestić, I.; Wieme, J.; Rogge, S. M. J.; Depauw, H.; Van Der Voort, P.; Vrielinck, H.; Van Speybroeck, V. Elucidating the vibrational fingerprint of the flexible metal−organic framework MIL-53(Al) using a combined experimental/computational approach. *J. Phys. Chem. C* **2018**, *122*, 2734−2746.
(48) Wieme, J.; Lejaeghere, K.; Kresse, G.; Van Speybroeck, V. Tuning the balance between dispersion and entropy to design

https://doi.org/10.1021/acsanm.3c00106
ACS Appl. Nano Mater. 2023, 6, 5645−5652

temperature-responsive flexible metal-organic frameworks. *Nat. Commun.* **2018**, *9*, 4899.
(49) Verploegh, R. J.; Wu, Y.; Sholl, D. S. Lattice-gas modeling of adsorbate diffusion in mixed-linker zeolitic imidazolate frameworks: effect of local imidazolate ordering. *Langmuir* **2017**, *33*, 6481−6491.
(50) Verploegh, R. J.; Wu, Y.; Boulfelfel, S. E.; Sholl, D. S. Quantitative Predictions of Molecular Diffusion in Binary Mixed-Linker Zeolitic Imidazolate Frameworks Using Molecular Simulations. *J. Phys. Chem. C* **2018**, *122*, 5627−5638.
(51) Han, R.; Ketkaew, R.; Luber, S. A concise review on recent developments of machine learning for the prediction of vibrational spectra. *J. Phys. Chem. A* **2022**, *126*, 801−812.

https://doi.org/10.1021/acsanm.3c00106
ACS Appl. Nano Mater. 2023, 6, 5645−5652